Asociación Argentina
de Mecánica Computacional

Mecánica Computacional Vol XXV, pp. 1127-1137
Alberto Cardona, Norberto Nigro, Victorio Sonzogni, Mario Storti. (Eds.)
Santa Fe, Argentina, Noviembre 2006

# A CONSERVATIVE HIGH-ORDER FINITE DIFFERENCE SCHEME FOR THE NUMERICAL SOLUTION OF THE LOW MACH-NUMBER EQUATIONS

**Omar D. Lopez, Robert Moser and Ofodike A. Ezekoye**

*Department of mechanical engineering, University of Texas at Austin, 1 University station C2200, Austin, TX 78712-0292. odlopez@mail.utexas.edu,* **http://www.me.utexas.edu**

**Keywords:** Conservative scheme, low-Mach number flows, high-order finite difference method, projection method.

**Abstract.** A spatially fourth order and temporally third order projection method is proposed for the numerical solution of the variable-density low-Mach-number approximation of the Navier-stokes equations. The algorithm is non-dissipative and kinetic energy conserving. These two characteristics are important in the simulation of turbulent flows, particularly turbulent reacting flows. Another important feature is that the equation of state is enforced exactly while enforcing the mass conservation constraint. The projection method requires that a variable coefficient Poisson equation has to be solved at every time step. Results from model problems will show the spatial and temporal convergence and also the performance of this algorithm in capturing the physics of the low Mach-number variable-density equations.

## 1 INTRODUCTION

Conservation of kinetic energy in numerical methods has become an important issue in large eddy simulation (LES) and direct numerical simulation (DNS) of turbulence. Kinetic energy conservation in a finite difference formulation is not a consequence of discrete momentum and discrete mass conservation, so conservation of kinetic energy has to be ensured through careful design of the finite difference operators. It is known that dissipative numerical schemes (e.g. up-winding) often introduce too much artificial damping for use in turbulence simulations, because the energy balance in turbulence is rather delicate. In the case of variable density flows, not conserving the kinetic energy can also lead to erroneous temperature and density fields. Much work has been done in the development of kinetic energy conservation algorithms for incompressible flows (see Vasilyev (2000); Gullbrand (2000); Morishini et al. (1998)), but there has been less work on variable density or compressible flows (see Nicoud (2000)).

In low-speed turbulent combustion applications, the low Mach-number, variable-density approximation of the Navier-Stokes equations is a good basis for simulation, as it supports large density variations while eliminating acoustic waves. This eliminates the need for extremely small time steps driven by the acoustics. This paper is organized as follows. Section 2 shows the equations that govern low Mach-number flows,and in section 3 some details of the numerical method and its implementation are shown. Finally, section 4 and 5 contain stability analysis of the scheme, some numerical results and convergence analysis of the method.

## 2 GOVERNING EQUATIONS

The low Mach-number approximation of the Navier-stokes equations is obtained as the low Mach-number asymptotic limit of the compressible Navier-Stokes equations in which temperature fluctuations are assumed to be of order 1. In this analysis, the pressure is expanded as:

$$P(x,t;M) = P_0(t) + M^2 P_2(x,t) + O(M^3) \tag{1}$$

In this expansion, $P_0$ is the spatially uniform thermodynamic pressure, and $P_2$ is the hydrodynamic pressure fluctuation. Details of the derivation of these equations can be found in Majda and Sethian (1985); Rehm and Baum (1978); Muller (1999). The final results of this process are the following equations (excluding the body forces):

*Conservation of mass:*

$$\frac{\partial \rho}{\partial t} + \frac{\partial \rho u_i}{\partial x_i} = 0 \tag{2}$$

*Momentum equation:*

$$\frac{\partial \rho u_i}{\partial t} + \frac{\partial \rho u_i u_j}{\partial x_j} = -\frac{\partial p}{\partial x_i} + \frac{1}{Re}\frac{\partial \tau_{ij}}{\partial x_i} \tag{3}$$

*Conservation of energy*

$$\rho C_p \left( \frac{\partial T}{\partial t} + u_j \frac{\partial T}{\partial x_j} \right) = \frac{1}{RePr}\frac{\partial q_j}{\partial x_j} + \frac{\gamma}{\gamma - 1}\frac{dP_0}{dt} \tag{4}$$

*Equation of state*

$$P_0 = \rho T \tag{5}$$

In equations 3 and 4, $Re$ and $Pr$ are the Reynolds and Prandtl number respectively; $\tau_{ij}$ and $q_j$ are the viscous stress tensor and the heat flux vector respectively; and $p = P_2$ is the hydrodynamic pressure fluctuation. The low Mach-number both eliminates the acoustic waves and reduces the number of dependent variables by one; this occurs because the energy equation reduces to a constraint, which can be derived by combining equations 2, 3 and 5 yielding:

$$\frac{\partial u_i}{\partial x_i} = \frac{1}{P_0 C_p}\left[\frac{1}{RePr}\frac{\partial}{\partial x_j}\left(k\frac{\partial T}{\partial x_j}\right) + \left(\frac{\gamma-1}{\gamma} - C_p\right)\frac{dP_0}{dt}\right] \tag{6}$$

For an open system, the thermodynamic pressure (Po) does not change in time, but in a closed system (sealed enclosure) the thermodynamic pressure can change in time. Notice that the source terms from the energy equation impact the mass conservation equation through the constraint 6.

## 3 NUMERICAL METHOD

Two general approaches to solving equations 2- 6 have appeared in the literature: the first approach consists in solving equations 2, 3, 5 and 6 so that, the energy equation is never explicitly solved but is accounted for through the constraint on the velocity divergence 6. This approach is used by McGrattan (2004) in the Fire Dynamic Simulator (FDS). The second and more common approach is to solve equations 2, 3, and 4, but in this case the equation of state is not satisfied exactly. This method has been used by Bell et al. (1998) and by Nicoud (2000).The former approach is pursued here.

### 3.1 Temporal discretization

A three-step hybrid Runge-Kutta/Crank-Nicolson (RK-CN) scheme was implemented for time advancement. This is essentially the scheme described in the Appendix of Moser et al. (1991). It's application to the low Mach-number equations is described here. In what follows, we describe a single substep of the scheme, since each substep is identical, except for the value of the coefficients. The superscript on the solution variables represents the subscript number (substep 0 is the result of the previous time step). Likewise, $\alpha_k, \gamma_k, \zeta_k$ and $\beta_k$ (k=1,2,3) represent the numerical parameters of the RK-CN scheme.

For each step, the conservation of mass equation (2) is advanced in time first as follows:

$$\rho^k = \rho^{k-1} - \Delta t\gamma_k\left(\frac{\partial \rho u_i}{\partial x_i}\right)^{k-1} - \Delta t\zeta_k\left(\frac{\partial \rho u_i}{\partial x_i}\right)^{k-2} \tag{7}$$

With $\rho^k$ known, the temperature at the next sub-step, $T_k$ can be determined from the equation of state (5), and then the divergence of the velocity $(\partial u_i/\partial x_i)^k$ is found from equation 6, to be used in the projection step below.

Now the momentum equation 3 is advanced in time. As in Moser et al. (1991), the linear terms are advanced implicitly while the non-linear terms are advanced explicitly:

$$\begin{aligned}\frac{\rho^k u_i^k - \rho^{k-1}u_i^{k-1}}{\Delta t} = {} & \alpha_k\left(-\frac{\partial P}{\partial x_i} + \frac{\partial \tau_{ij}}{\partial x_j}\right)^{k-1} + \beta_k\left(-\frac{\partial P}{\partial x_i} + \frac{\partial \tau_{ij}}{\partial x_j}\right)^{k} - \cdots \\ & - \gamma_k\left(\frac{\partial \rho u_i u_j}{\partial x_j}\right)^{k-1} - \zeta_k\left(\frac{\partial \rho u_i u_j}{\partial x_j}\right)^{k-2}\end{aligned} \tag{8}$$

Now, applying the projection method (see Chorin (1968)) on equation 8 leads to a decomposition (Hodge decomposition) of the velocity into a solenoidal field and the gradient of a scalar.

Equation 9 show the result of this decomposition:

$$\begin{aligned}\frac{\rho^k \hat{u}_i^k - \rho^{k-1} u_i^{k-1}}{\Delta t} &= -(\alpha_k + \beta_k)\frac{\partial P^{k-1}}{\partial x_i} + \alpha_k \frac{\partial \tau_{ij}^{k-1}}{\partial x_j} + \beta_k \frac{\partial \hat{\tau}_{ij}^{k}}{\partial x_j} - \gamma_k \left(\frac{\partial \rho u_i u_j}{\partial x_j}\right)^{k-1} - \cdots \\ &\quad - \zeta_k \left(\frac{\partial \rho u_i u_j}{\partial x_j}\right)^{k-2} \\ \frac{\rho^k u_i^k - \rho^k \hat{u}_i^k}{\Delta t} &= -\beta_k \frac{\partial \delta P^k}{\partial x_i}\end{aligned} \tag{9}$$

Where, the advancement substep has been split into two fractional steps. The intermediate velocity $(\hat{u}_i^k)$ is known from the first fractional step. Then to enforce the constraint on the velocity divergence, a variable coefficient Poisson equation (equation 10) is solved every substep, using the PETSc library (see Balay et al. (2001), Balay et al. (2004)).

$$\frac{\partial}{\partial x_j}\left(\frac{1}{\rho^k}\frac{\partial \delta P^k}{\partial x_j}\right) = \frac{1}{\beta_k \Delta t}\left(\frac{\partial \hat{u}_j^k}{\partial x_j} - \frac{\partial u_j^k}{\partial x_j}\right) \tag{10}$$

where $\partial u_j^k / \partial x_j$ is known from the constraint. The velocity is corrected using 9, and $P^k = P^{k-1} + \delta P^k$, and the solution at the next time step is obtained after the third substep.

### 3.2 Spatial discretization

The spatial scheme is designed for use on a regular staggered Cartesian mesh. Several fourth-order derivative and interpolation operators are needed, which are defined in terms of the simple second order operators below (see Morishini et al. (1998) and Nicoud (2000) for more details):

$$\overline{\phi}^{nx_i} = \frac{\phi(x_i + n\Delta x_i/2) + \phi(x_i - n\Delta x_i/2)}{2} \tag{11}$$

$$\frac{\delta_n \phi}{\delta_n x_i} = \frac{\phi(x_i + n\Delta x_i/2) - \phi(x_i - n\Delta x_i/2)}{n\Delta x_i} \tag{12}$$

From these operators, the terms of the Navier-Stokes equations can be discretized (see Nicoud (2000)). As an example, the convection term in the momentum equations is approximated:

$$\begin{aligned}\frac{\partial \rho u_i u_j}{\partial x_j} &= \frac{9}{8}\frac{\delta_1}{\delta_1 x_j}\left[\left(\frac{9}{8}\overline{\rho^{(4j)} u_j}^{1x_i} - \frac{1}{8}\overline{\rho^{(4j)} u_j}^{3x_i}\right)\overline{u_i}^{1x_j}\right] - \cdots \\ &\quad - \frac{1}{8}\frac{\delta_1}{\delta_1 x_j}\left[\left(\frac{9}{8}\overline{\rho^{(4j)} u_j}^{1x_i} - \frac{1}{8}\overline{\rho^{(4j)} u_j}^{3x_i}\right)\overline{u_i}^{3x_j}\right]\end{aligned} \tag{13}$$

Where:
$\rho^{(4j)} = \frac{9}{8}\overline{\rho}^{1x_j} - \frac{1}{8}\overline{\rho}^{3x_j}$ is a fourth order interpolation of the density.

In the current paper, we consider only periodic boundary conditions, which require no special discretization. For a discussion of wall boundary treatments in similar schemes, see Morishini et al. (1998).

## 4 STABILITY ANALYSIS

The time discretization used in this method reduces to a third order Runge-Kutta (RK3) scheme for a pure convection problem. It is known that a RK3 scheme has a theoretical CFL limit of $\sqrt{3}$ and the stability region shown in figure 1. But according to Moser et al. (1991) in practice (for a RK/CN scheme) CFL can go up to 2 due to the help of viscous terms and the intermittency of the high velocity conditions.

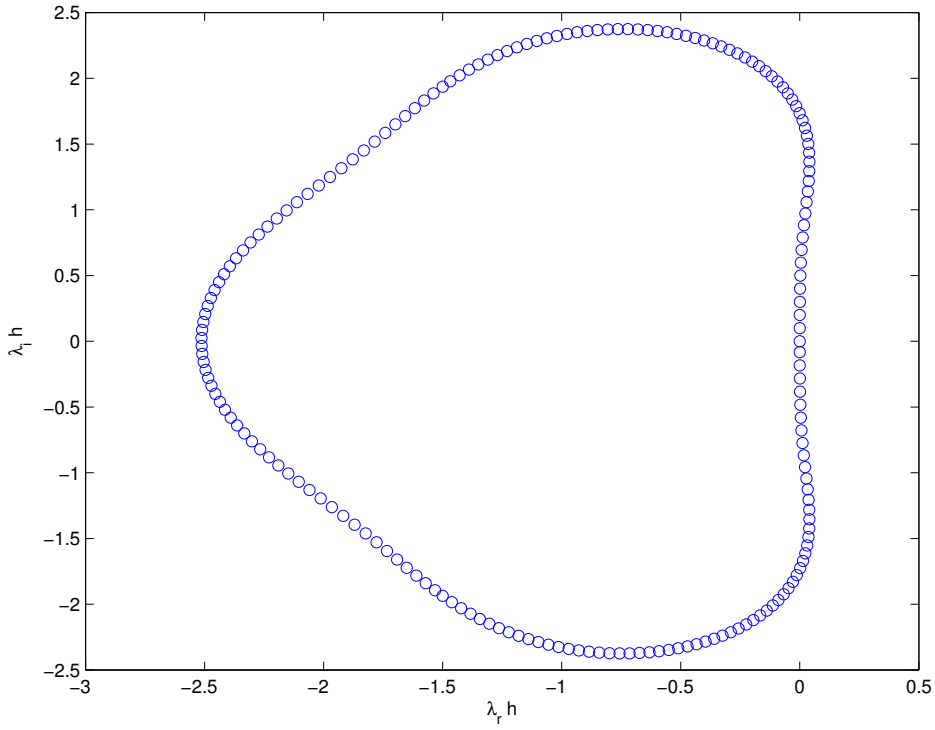


Figure 1: Stability region for a pure convective problem

In order to get a better idea of the stability properties of the numerical scheme described in section 3, a Von Neumann stability analyisis was performed on the linear 1D convection diffusion equation.

$$\frac{\partial u}{\partial t} + c\frac{\partial u}{\partial x} = \nu\frac{\partial^2 u}{\partial x^2} \tag{14}$$

Using the fourth order operators described in section 3.2, it is possible to derive equation 15 for the error $(\epsilon)$ at the first substep of the RK/CN scheme

$$\epsilon = \frac{\frac{Fo\alpha_1}{288}\left(-730 + 783\cos(\omega h) - 54\cos(2\omega h) + \cos(3\omega h)\right) - \frac{i\gamma_1 CFL}{24}\left(27\sin 3\omega h - \sin\omega h\right)}{1 - \frac{Fo\beta_1}{288}\left(-730 + 783\cos(\omega h) - 54\cos(2\omega h) + \cos(3\omega h)\right)} \tag{15}$$

Where:
h is the grid spacing i.e. $\Delta x$
CFL is the Courant-Freidricks-Levy number defined as $\frac{c\Delta t}{h}$
Fo is the Fourier number defined as $\frac{\nu\Delta t}{h^2}$

The locus of $\epsilon$ for different values of CFL with Fo=0.1 is shown in figure 2. For pure diffusion problems the scheme is unconditionally stable, but for pure convective problems is conditionally unstable. As it is known this stability is determined by the CFL number which it was found to be critical at 1.6.

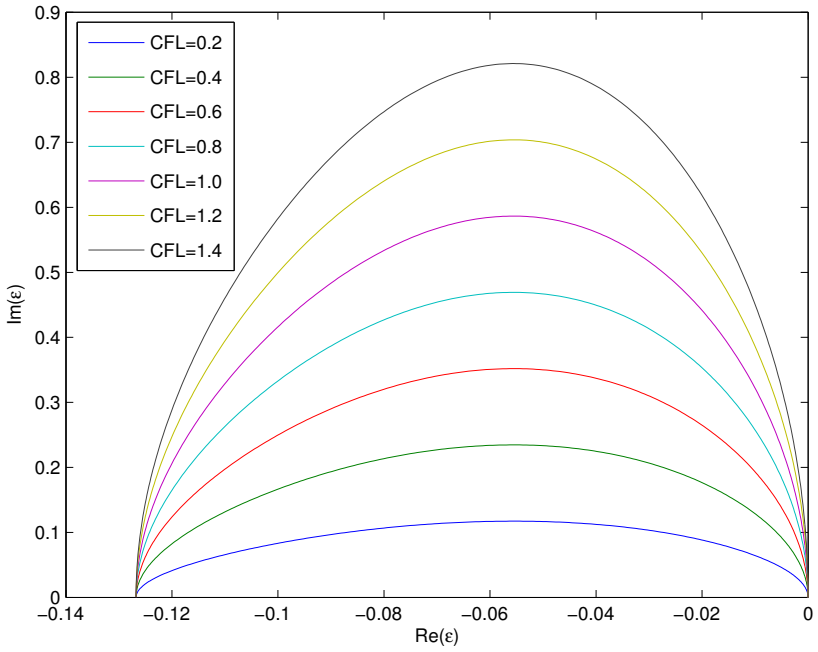


Figure 2: Locus of $\epsilon$ for Fo=0.1

## 5 NUMERICAL RESULTS

Three numerical experiments were performed in order to test the numerical scheme and its implementation. First, a 1D convection-diffusion problem was set to test spatial and temporal convergence in a variable density case. Second, a 2D inviscid solenoidal velocity field was used to test kinetic energy conservation. Finally, a 2D constant and variable density problem was used to test spatial and temporal convergence.

### 5.1 Spatial and temporal convergence in 1D

The test problem for this experiment is a temperature profile that will be convected in the $x$-direction. For simplicity the flow was assumed to be inviscid and the domain was the interval [0,1]. The initial temperature profile is a Gaussian given by equation 16.

$$T(K) = 293 + 50 \exp\left[-\left(\frac{x - 0.5}{0.05}\right)^2\right] \tag{16}$$

The velocity in the $x$-direction ($u$) was set equal to 1, the hydrodynamic pressure was set to 0 Pa and the thermodynamic pressure was set to 1. The working fluid was assumed to be air so that its thermal conductivity (k) could be estimated from polynomial correlations. Since the thermal diffusivity of air is O($1 \times 10^{-5}$), the global Peclet number is very high O($1 \times 10^{5}$). For the spatial

convergence the grid was changed from 100, 200, 400 to 800 nodes while the time step was held in 0.00125 so that the CFL number changed from 0.125 to 1. For the temporal convergence the mesh was held in 100 grid points and the time was change from 0.005 to 0.000625 so that the CFL number changed from 0.5 to 0.0625. Figure 3. shows the profile of velocity at t=1 for four different time steps. The velocity induced by the diffusion process was of the order $1 \times 10^{-6}$. The shape of the $u$-velocity profile is in agreement with the theory and what is expected from equation 6. Table 1 summarizes the numerical results from this experiment.

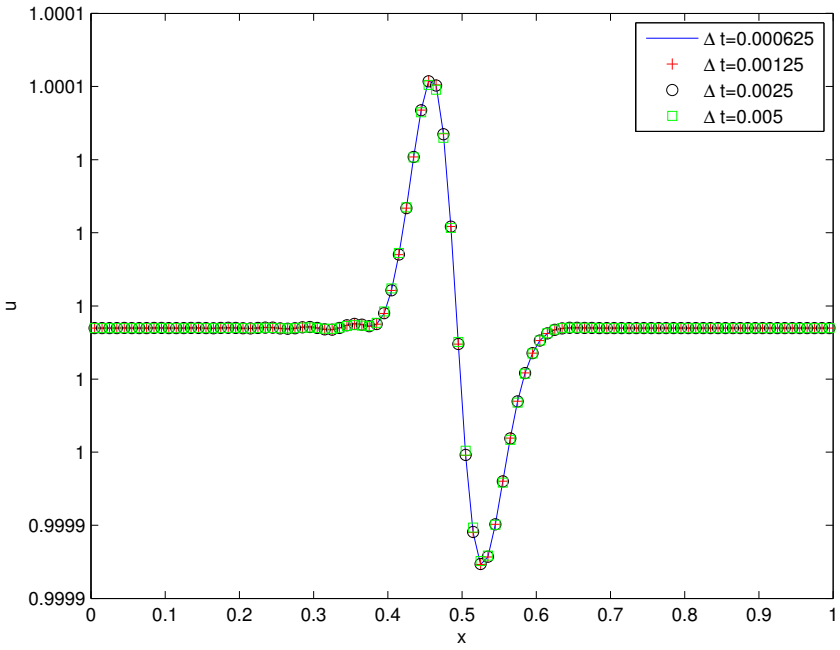


Figure 3: $u$ velocity profile

| | u | v | T |
|---|---|---|---|
| Spatial | 3.971 | 3.954 | 3.881 |
| Temporal | 2.967 | 2.942 | 2.977 |

Table 1: Spatial and temporal convergence rates

## 5.2 Kinetic energy conservation

For this numerical experiment a 2-dimensional rectangular domain [0,1]x[0,1] is used, with an initial steady state solenoidal velocity field given by equation 17

$$\begin{aligned} u(x,y) &= -\cos(2\pi x)\sin(2\pi y) \\ v(x,y) &= \sin(2\pi x)\cos(2\pi y) \end{aligned} \tag{17}$$

The temperature field was set as a Gaussian random field with a mean value of 397 K and a root mean square fluctuation of 57 K. The density field can be computed from the equation of state. Using equation 17 and the initial random density field, the initial kinetic energy can be

computed ($KE_o = 0.2274J$). A mesh of $24 \times 24$ points was used, so that $\Delta x = \Delta y = 4.2e-2$. According to Nicoud (2000), the integration time for this numerical experiment is given by equation 18

$$t = \frac{0.125L}{\sqrt{KE_o}} = 0.3125s \tag{18}$$

Table 2 and figure 4 show the results for this experiment. It is evident that the scheme conserves global kinetic energy, so that the divergence-free constraint is recovered in the inviscid limit.

| $\Delta t$ | CFL | $KE_o$ | $KE_f$ | ERROR |
|---|---|---|---|---|
| 0.04166 | 1 | 0.2274 | 0.226879 | $2.59 \times 10^{-3}$ |
| 0.02083 | 0.5 | 0.2274 | 0.226891 | $2.54 \times 10^{-3}$ |
| 0.004166 | 0.1 | 0.2274 | 0.226918 | $2.42 \times 10^{-3}$ |
| 0.002083 | 0.05 | 0.2274 | 0.226921 | $2.40 \times 10^{-3}$ |
| 0.0004166 | 0.01 | 0.2274 | 0.226927 | $2.38 \times 10^{-3}$ |

Table 2: Numerical results from KE conservation.

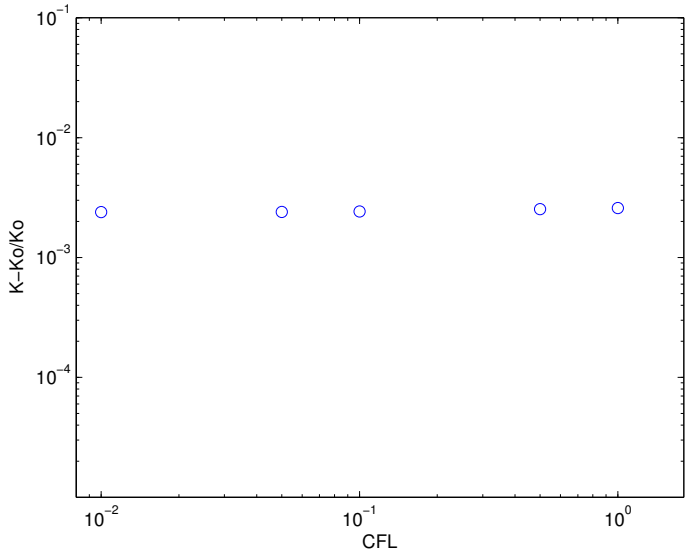


Figure 4: Error of the KE as a function of CFL

The error in table 1 was calculated using the ratio between the difference in the initial and final kinetic energy i.e.

$$ERROR = \frac{KE_o - KE_f}{KE_o} \tag{19}$$

### 5.3 Spatial and temporal convergence in 2D

The primary objective of this experiment is to test the fourth order convergence in space and the third order convergence in time. There are two different study cases: the constant density case and the variable density case.

### 5.3.1 Constant density

In this test, we evaluate the solution of the Euler equations as a first approximation of the Navier-Stokes equations. This can be done by assuming a constant density field and a solenoidal velocity field in a $2\pi \times 2\pi$ domain as follows:

$$\begin{aligned} u(x, y, t = 0) &= 1 - 2\cos x \sin y \\ v(x, y, t = 0) &= 1 + 2\sin x \cos y \end{aligned} \tag{20}$$

This initial condition has an exact solution that corresponds to diagonally translating vortices which is given by equation 21:

$$\begin{aligned} u(x, y, t) &= 1 - 2\cos(x - t)\sin(y - t) \\ v(x, y, t) &= 1 + 2\sin(x - t)\cos(y - t) \\ P(x, y, t) &= -\cos(2(x - t)) - \cos(2(y - t)) \end{aligned} \tag{21}$$

Four different meshes were used ($12 \times 12$, $24 \times 24$, $48 \times 48$ and $96 \times 96$) to study the spatial convergence. Table 3 shows the result from these numerical experiments. As one can see, the method is fourth order in space for both velocity and pressure. For the temporal convergence, a $24 \times 24$ mesh was used and the time step was changed from 0.01 to 0.00125 meaning CFL number between 0.72 and 0.18. Table 3 and figure 5 show the results from this study, it is noticed that the scheme is third order in time for the velocity but the numerical results showed that for the pressure, first order accuracy was achieved. This is expected, and is a consequence of the operator splitting performed in the projection method (see Perot (1993) and Chorin (1969)). Figure 6 shows the u velocity contours (numerical solution) at t=1 s.

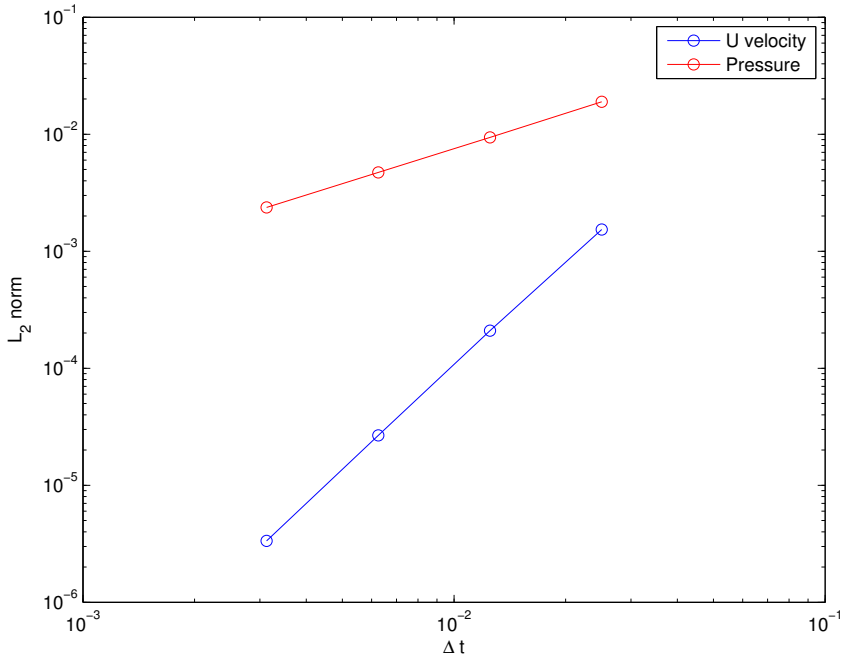


Figure 5: Temporal convergence (2D constant density case).

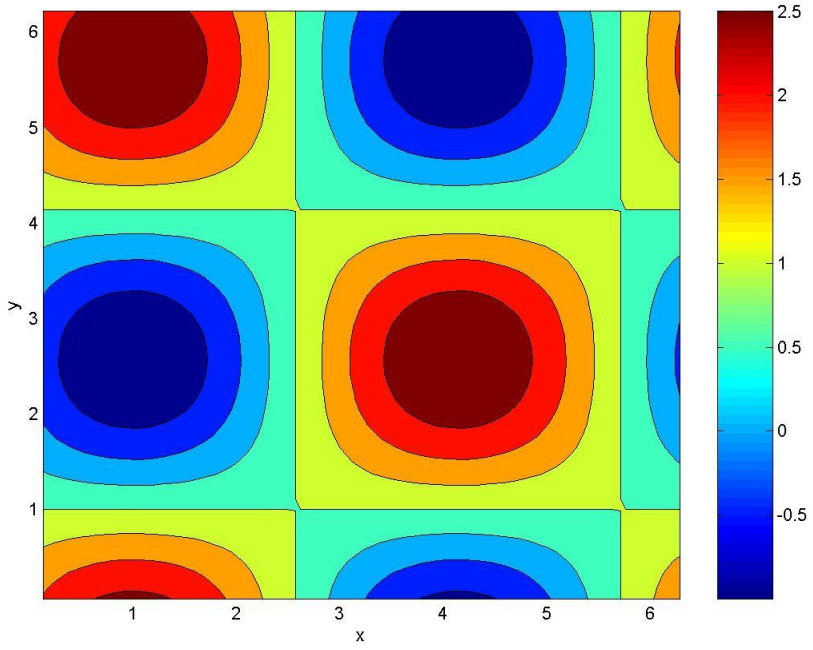


Figure 6: Contour plot of u at t=1 s

| | u | v | p |
|---|---|---|---|
| Spatial | 3.956 | 3.978 | 3.879 |
| Temporal | 2.949 | 2.967 | 0.998 |

Table 3: Spatial and temporal convergence rates

### 5.3.2 Variable density

The initial condition for this numerical test is given by equation 22, assuming that the thermal conductivity (K) is constant.

$$
\begin{aligned}
u(x,y,t=0) &= -\cos x \sin y + \frac{100KR}{C_p P_0} \sin x \cos y \\
v(x,y,t=0) &= -\cos y \sin x + \frac{100KR}{C_p P_0} \sin y \cos x \\
T(x,y,t=0) &= 293 - 100 \cos x \sin y
\end{aligned}
\tag{22}
$$

Notice that the constraint on the velocity field (equation 6) is satisfied by this initial condition. The configuration used to test the spatial and temporal accuracy was exactly the same as that used in the previous section (see section 4.3.1). Results are summarized in table 4

| | u | v | p | T | $\rho$ |
|---|---|---|---|---|---|
| Spatial | 3.956 | 3.978 | 3.879 | 3.921 | 3.913 |
| Temporal | 2.949 | 2.967 | 0.998 | 2.956 | 2.944 |

Table 4: Spatial and temporal convergence rates (variable density case)

## 6 CONCLUSIONS

Higher-order schemes, as proposed by Morishini et al. (1998), can be extended to low Mach-number variable density flows while preserving their conservative properties. Using the constraint on the velocity divergence, instead of advancing the energy equation, is an attractive numerical technique for solving the low Mach-number approximation since it allows exact satisfaction of the equation of state. As pointed out by Nicoud, the variable coefficient Poisson equation plays an important role in the numerical scheme for the solution of low Mach-number flows, since it ensures the correct constraint in the velocity field. Though in the examples shown in this paper, $P_0$ was always a constant this algorithm can be extended to problems in which $P_0$ depends on time, by integrating the equation of state.

## REFERENCES


Satish Balay, Kris Buschelman, Victor Eijkhout, William D. Gropp, Dinesh Kaushik, Matthew G. Knepley, Lois Curfman McInnes, Barry F. Smith, and Hong Zhang. PETSc users manual. Technical Report ANL-95/11 - Revision 2.1.5, ANL, 2004.

Satish Balay, Kris Buschelman, William D. Gropp, Dinesh Kaushik, Matthew G. Knepley, Lois Curfman McInnes, Barry F. Smith, and Hong Zhang. PETSc Web page, 2001. http://www.mcs.anl.gov/petsc.

J.B. Bell, P. Colella, A.S. Almgren, L.H. Howell, and M.L. Welcome. A conservative adaptive projection method for the variable density incompressible navier-stokes equations. *Journal of Computational Physics*, 142:1–46, 1998.

A. Chorin. Numerical solution of the navier-stokes equations. *Mathematics of computation*, 22: 745–762, 1968.

A. Chorin. On the convergence of discrete approximations of the navier-stokes equations. *Mathematics of computation*, 23:341–353, 1969.

J. Gullbrand. An evaluation of a conservative fourth order dns code in turbulent channel flow. *Annual research briefs, CTR, NASA Ames/Stanford University*, pages 211–218, 2000.

A. Majda and J Sethian. The derivation and numerical solution of the navier-stokes equations for zero mach number combustion. *Combustion Science and Technology*, 42:185, 1985.

K.B. McGrattan. *Fire Dynamics Simulator (Version 4) Technical guide*. National Institute of Standards and Technology, 2004.

Y. Morishini, T. Lund, O. Vasilyev, and P. Moin. Fully conservative higher order finite difference schemes for incompressible flow. *Journal of Computational Physics*, 143:90–124, 1998.

R. Moser, P.R. Spalart, and M. Rogers. Spectral methods for the navier-stokes equations with one infinite and two periodic directions. *Journal of Computational Physics*, 96:297–324, 1991.

B. Muller. Low mach number asymptotics of the navier-stokes equation and numerical implications. *Von Karman institute for fluid dynamics lecture series*, 3, 1999.

F. Nicoud. Conservative higher-order finite-difference scheme for low-mach number flows. *Journal of Computational Physics*, 158:71–97, 2000.

J. B. Perot. An analysis of the fractional step method. *Journal of Computational Physics*, 108: 51–58, 1993.

R. Rehm and H. Baum. The equations of motion for thermally driven, bouyant flows. *Journal of research of the NBS*, 83, 1978.

O. V. Vasilyev. Higher order finite difference schemes on non-uniform meshes with good conservation properties. *Journal of Computational Physics*, 157:746–761, 2000.